THE JOURNAL OF BIOLOGICAL CHEMISTRY VOL. 286, NO. 2, pp. 1189–1195, January 14, 2011

Crystal Structure of Staphylococcal Enterotoxin G (SEG) in Complex with a Mouse T-cell Receptor β Chain*

Received for publication, May 10, 2010, and in revised form, September 20, 2010 Published, JBC Papers in Press, November 8, 2010, DOI 10.1074/jbc.M110.142471

Marisa M. Fernández[‡§], Sangwoo Cho[§], Mauricio C. De Marzi[‡¶], Melissa C. Kerzic[§], Howard Robinson[‖], Roy A. Mariuzza[§1], and Emilio L. Malchiodi[‡§2]

From the [‡]Cátedra de Inmunología and Instituto de Estudios de la Inmunidad Humoral Prof. Ricardo A. Margni, Consejo Nacional de Investigaciones Científicas y Técnicas, Facultad de Farmacia y Bioquímica, Universidad de Buenos Aires, Junín 956 4to P, 1113 Buenos Aires, Argentina, the [§]W. M. Keck Laboratory for Structural Biology, University of Maryland Institute for Bioscience and Biotechnology Research, Rockville, Maryland 20850, [¶]Departamento de Ciencias Básicas, Universidad Nacional de Luján, Ruta 5 y Constitución, 6700 Luján, Buenos Aires, Argentina, and [‖]Department of Biology, Brookhaven National Laboratory, Upton, New York 11973

Superantigens (SAgs) are bacterial or viral toxins that bind MHC class II (MHC-II) molecules and T-cell receptor (TCR) in a nonconventional manner, inducing T-cell activation that leads to inflammatory cytokine production, which may result in acute toxic shock. In addition, the emerging threat of purpura fulminans and community-associated meticillin-resistant *Staphylococcus aureus* emphasizes the importance of a better characterization of SAg binding to their natural ligands that may allow the development of reagents to neutralize their action. The three-dimensional structure of the complex between a mouse TCR β chain (mVβ8.2) and staphylococcal enterotoxin G (SEG) at 2.0 Å resolution revealed a binding site that does not conserve the "hot spots" present in mVβ8.2-SEC2, mVβ8.2-SEC3, mVβ8.2-SEB, and mVβ8.2-SPEA complexes. Analysis of the mVβ8.2-SEG interface allowed us to explain the higher affinity of this complex compared with the others, which may account for the early activation of T-cells bearing mVβ8.2 by SEG. This mode of interaction between SEG and mVβ8.2 could be an adaptive advantage to bestow on the pathogen a faster rate of colonization of the host.

Superantigens (SAgs)[3] are bacterial toxins or viral proteins that bind simultaneously as unprocessed molecules the T-cell receptor (TCR) and MHC-II molecules. As a consequence of this interaction, SAgs activate large numbers of T-cells, promoting a massive release of inflammatory cytokines, such as IL-1, IL-2, TNF-α, and TNF-β. These host cytokines are believed to be responsible for the most severe consequences of SAg intoxication, including capillary leak, renal failure, acute respiratory distress, and death. Systemic intoxication by SAgs can lead to a severe condition known as toxic shock syndrome (reviewed in Ref. 1), which is an acute, multisystem, toxin-mediated illness, often resulting in multiorgan failure. Toxic shock syndrome represents the most devastating expression of a spectrum of diseases caused by SAg-producing strains of *Staphylococcus aureus* and *Streptococcus pyogenes* (reviewed in Ref. 2). Bacterial SAgs have also been identified as category B agents of bioterrorism by the U. S. Centers for Disease Control and Prevention due to their extreme virulence and the ease with which they can be produced and disseminated.

Most of the known SAgs share a characteristic three-dimensional structure and bind MHC-II outside of the peptide-binding groove (3–10). However, the complexes formed between SAgs and MHC-II molecules display diversity and the interaction can be through either the α or β chain contacting or not the antigenic peptide (11–15). On the other hand, the binding to the TCR is not yet so well characterized due to the few TCR-SAg complexes that have been crystallized (16–19).

SAgs have been classified into five evolutionary groups or families based on their amino acid sequence (20). All members of group II, or the SEB family, which include SAgs from *S. pyogenes* SPEA and SSA and *S. aureus* SAgs SEB and SEC1–3 are known to interact with the mouse TCR Vβ8.2 (mVβ8.2) chain. Because mVβ8.2 was described as the principal TCR involved in experimental autoimmune encephalitis, and taking into account the potential role of SAgs in autoimmune diseases (21–23), it is important to analyze the binding of SAgs that stimulate T-cells carrying this particular β chain. Four members of this family, SEB, SEC2, SEC3, and SPEA, have been crystallized in complex with mVβ8.2, allowing detailed characterization of this interaction. The binding mode

* This work was supported, in whole or in part, by National Institutes of Health Grants AI36900 and AI073654. This work was also supported by Agencia Nacional de Promoción Científica y Técnica Grant PICT 38293 (to E. L. M.) and 450 (to M. M. F.); and National Multiple Sclerosis Society Grant RG2747 (to R. A. M.). Financial support for use of the National Synchrotron Light Source comes principally from the Offices of Biological and Environmental Research and of Basic Energy Sciences of the U. S. Department of Energy and from the National Center for Research Resources of the National Institutes of Health.

The atomic coordinates and structure factors (codes 3MC0 and 3OWE) have been deposited in the Protein Data Bank, Research Collaboratory for Structural Bioinformatics, Rutgers University, New Brunswick, NJ (http://www.rcsb.org/).

[1] To whom correspondence may be addressed: 9600 Gudelsky Dr., Rockville, MD 20850. Tel.: 240-314-6243; Fax: 240-314-6255; E-mail: mariuzza@carb.nist.gov.

[2] Supported by the Fogarty International Center (TW007972) and International Centre for Genetic Engineering and Biotechnology (CRP/ARG09-02). To whom correspondence may be addressed: Junín 956 4to P, 1113 Buenos Aires, Argentina. Tel.: 5411-4964-8259; Fax: 5411-4964-0024; E-mail: emalchio@ffyb.uba.ar.

[3] The abbreviations used are: SAg, superantigens; TCR, T-cell receptor; SEB, staphylococcal enterotoxin B; SEC, staphylococcal enterotoxin C; SEU, staphylococcal enterotoxin U; SSA, streptococcal superantigen A; SPEA, streptococcal pyrogenic enterotoxin A; SEG, staphylococcal enterotoxin G; mVβ8, mouse TCR β chain; r.m.s., root mean square; CDR, complementary determining region; HV4, hypervariable region 4.

to mVβ8.2 is strictly conserved among the members of the SEB family and occurs through the variable region of the TCR β chain, contacting complementary determining region (CDR) 2, frameworks regions (FR) 2 and 3 and hypervariable region 4 (HV4) (17, 18). The streptococcal SAg SPEA also contacts CDR1 (19). In addition to the crystal structures, an extensive biophysical analysis of SAg mutants identified the energetic hot spots in binding to mVβ8.2 (24).

The SAgs from *S. aureus* SEG and SEU are the latest to be included in the SEB family (20). SEG was identified by Munson *et al.* (25) and is contained in the *egc* enterotoxin gene cluster with other four SAgs (26). SEG is 233-residues-long, corresponding to a mature protein of 27 kDa, which shares 41 to 46% amino acid sequence identity with other members of the SEB family. SEG has being implicated in toxic shock syndrome and scarlet fever associated with infecting *S. aureus* strains that lack genes for the classical members of the pyrogenic toxin SAg, comprising genes *sea-see* and the *tsst-1* (27). In addition, recent reports showed a higher frequency of *seg* than the classical genes in *S. aureus* isolated from several sources (28, 29).

We recently reported that, *in vivo*, SEG stimulates mouse T-cells carrying Vβ7 and Vβ9 TCRs. Stimulation reached a maximum at day 4 or later after injection (30), as usually happens with T-cells stimulated by SEC2–3 or SEB (31, 32). Surprisingly, we also found that SEG stimulates an earlier, stronger, and more widespread stimulation of mVβ8.2-bearing T-cells, compared with other members of the SEB family, which reached a maximum at day 2 instead of day 4 or later (30). In addition, we analyzed SEG binding to mVβ8.2 by surface plasmon resonance and isothermal titration calorimetry, which yielded similar results. The affinity (K_D = 0.125 μM by isothermal titration calorimetry and 0.270 μM by surface plasmon resonance) is the highest reported for an interaction of a wild-type SAg and a TCR (33). Sequence alignment of SEB family members revealed that SEG has changes in three highly conserved key amino acid positions, N58S, Y88F, and Q206P (SEG numbering), that were predicted to contact mVβ8.2. The crystal structure of SEG in unbound form (33) suggested that deletions in the sequence and natural mutations of hot spot residues are responsible for structural remodeling of the putative TCR-binding surface but could not explain the high affinity mentioned above. We also analyzed SEG binding to a mutant of mVβ8.2 (designated L2CM) that displays high affinity for SEC3 (33, 34). We found that the mutated residues responsible for the increased affinity of L2CM for SEC3, as well as SSA, did not greatly improve the affinity for SEG (33). Here, we describe the crystal structure of SEG bound to mVβ8.2 and L2CM and compare these structures with those of other SAgs bound to mVβ8.2.

EXPERIMENTAL PROCEDURES

Production and Purification of SAgs—The cloning of SEG was described previously (30). Briefly, *Escherichia coli* BL1(DE3) cells were transformed with *seg* cloned into the NcoI and BamHI sites of the pET22b expression vector. For expression of C-terminal His_6-tagged SEG mature protein, BL21 cells were grown in LB medium/ampicillin 100 μg/ml at 30 °C and induced with 0.2 mM IPTG at an A_{600} of 1. SEG was expressed as a soluble protein in the bacterial periplasmic space and released by osmotic shock, using Tris-EDTA-sucrose buffer. Soluble SEG was purified using a Ni^{2+}-nitrilotriacetic acid column.

Recombinant TCR β Chains—The cloning of mouse TCR β chain mVβ8.2 and the high affinity mutant LC2M was described previously (34). Briefly, Vβ8.2 and LC2M were cloned into expression vector pT7–7 and expressed as inclusion bodies in *E. coli* BL21(DE3). The inclusion bodies were washed three times with 50 mM Tris-HCl (pH 8.0), 0.1 M NaCl, 2 mM EDTA, and 0.5% Triton X-100, and another three times with the same buffer without Triton X-100, and then solubilized in 50 mM Tris-HCl (pH 8.0), 8 M urea, 2 mM EDTA, and 1 mM DTT. For *in vitro* folding, solubilized TCR was diluted to a final concentration of 20–50 μg/ml into 1.0 M arginine, 50 mM Tris-HCl (pH 8.5), 2 mM EDTA, 5 mM cysteamine and 0.5 mM cystamine. After 3 days at 4 °C, the folding mixture was concentrated, dialyzed against 50 mM Tris-HCl (pH 8.5), and applied to a Mono Q anion exchange column (Amersham Biosciences) equilibrated in the same buffer. The protein was eluted with a linear NaCl gradient. Further purification was carried out by size exclusion using a Superdex 75 HR column (Amersham Biosciences) in PBS.

Data Collection—Purified proteins were dialyzed against PBS and mixed in an equimolar ratio for further complex purification by size exclusion chromatography. The exclusion volume containing the complex was concentrated to 7.5 mg/ml of protein prior to dialysis against 0.01 M HEPES (pH 7) and 0.02 M NaCl. Crystallization trials on the SEG-Vβ8.2 and SEG-L2CM complexes were carried out in hanging drops at an initial protein concentration of 3.25 mg/ml in the drop, by mixing 2 μl each of protein solution and mother liquor. Crystals of the SEG-Vβ8.2 and SEG-L2CM complexes grew at room temperature in 1.4 M sodium acetate, 0.1 M sodium cacodylate (pH 6.5), and 0.2 M sodium citrate, 30% isopropanol and 0.1 M sodium cacodylate (pH 6.5), respectively. SEG-Vβ8.2 and SEG-L2CM crystals were transferred to mother liquor containing 10% (v/v) glycerol and frozen in liquid nitrogen. Diffraction data to 2.6 and 2.8 Å resolutions, respectively, were obtained at 100 K on an R-axis IV^{2+} image plate detector (Rigaku). Higher resolution data (2.0 and 2.6 Å, respectively) were collected using synchrotron radiation at beamline X-25 of the National Synchrotron Light Source, and were processed using the programs DENZO and SCALEPACK (35).

Structure Determination and Refinement—The SEG-Vβ8.2 and SEG-L2CM complex structures were determined by molecular replacement using the program Molrep in the CCP4 program suite (36) with the SEC3-Vβ8.2 and SEC3-L2CM complex structures (Protein Data Bank codes 1JCK and 2AQ3, respectively) (17, 37) as search models. Two SEG-Vβ8.2 and eight SEG-L2CM complexes were found in the asymmetric unit with a Matthews coefficient of 3.65 $Å^3$/Da and 4.03 $Å^3$/Da, respectively (solvent content ~65 and ~70%, respectively). Initial refinement was performed using CNS with positional, simulated annealing and individual B factor refinement. Manual model rebuilding was carried out iteratively in XtalView (38) using σ_A-weighted $2F_o$-F_c maps. After CNS refinement converged, further refinement was carried out with Ref-

mac5 (39), during which solvent molecules were placed in >2σ peaks in the σ_A-weighted $2F_o - F_c$ maps with regard to potential interactions with hydrogen bonding partners. Data collection and refinement statistics are summarized in Table 1.

RESULTS AND DISCUSSION

Overall Structure of mVβ8.2-SEG Complex—We determined the structure of the complex between SEG and the mVβ8.2 chain to 2.0 Å resolution (Table 1). There are two SEG and two mVβ8.2 molecules in the asymmetric unit. All the regions of the complex are well ordered, with only the β4–β5 loop of SEG lacking electron density. SEG appears to be less ordered than the Vβ domain, as reflected by higher mean temperature (B) factors. Although two complexes are present in the asymmetric unit, their superposition does not indicate significant differences (0.26 and 0.15 Å for the Vβ chain and SEG, respectively). In addition, the same set of hydrogen bonds is observed, the van der Waals contacts involve the same residues, and the buried surface in both complexes exhibit no significant differences.

TABLE 1
Data collection and refinement statistics

	SEG/Vβ8.2	SEG/L2CM
Space group	$P3_121$	$P43$
Unit cell dimensions (Å)	a = 91.19, b = 91.19, c = 233.40	a = 141.21, b = 141.21, c = 255.75
Resolution (Å)	78.9-2.0	50.0-2.6
Observations	867,481	2,149,930
Unique reflections	68,345 (3142)[a]	144,940 (10,462)[a]
Completeness (%)	93.7 (60.5)	99.7 (97.2)
R_{merge} (%)[b]	8.4 (21.6)	11.1 (53.1)
R_{cryst} (%)[c]	19.5 (22.3)	21.1 (30.6)
R_{free} (%)[d]	21.1 (27.7)	26.1 (39.2)
Molecules per asymmetric unit	2 × SEG/2 × Vβ8.2	8 × SEG/8 × L2CM
Protein residues	673	2784
No. of acetates	8	
No. of water molecules	490	186
Average B factors (Å^2)		
SEG	35.9	30.8
Vβ8.2	30.2	41.6
Acetate	45.4	
Waters	40.9	24.2
r.m.s.d.		
Bonds (Å)	0.032	0.032
Angles	2.42°	2.66°
Ramachandran plot statistics (%)		
Core	90.2	85.9
Allowed	9.1	12.8
Generous	0.5	0.7
Disallowed	0.2	0.6

[a] Values in parentheses correspond to the highest resolution shell (1.99–2.05 Å for SEG/Vβ8.2 and 2.60–2.67 for SEG/L2CM).
[b] $R_{merge}(I) = (\Sigma|I(i) - \langle I(h)\rangle|/\Sigma I(i))$, where $I(i)$ is the ith observation of the intensity of the *hkl* reflection, and $\langle I\rangle$ is the mean intensity from multiple measurements of the *hkl* reflection.
[c] $R_{cryst}(F) = \Sigma_h||F_{obs}(h)| - |F_{calc}(h)||/\Sigma_h|F_{obs}(h)|$, and $|F_{calc}(h)|$ are the observed and calculated structure factor amplitudes for the *hkl* reflection.
[d] R_{free} is calculated over reflections in a test set not included in atomic refinement: 3634 reflections, 5.0% for SEG/Vβ8.2; and 7666 reflections, 5.0% for SEG/L2CM.

The overall structure of the mVβ8.2-SEG complex is shown in Fig. 1*A*. The complex is formed through contacts between CDR2 and FR2 and -3 of the variable domain of the mVβ8.2 chain, which binds in the cleft between the small and large domains of SEG. Although SEG does not contact HV4 of mVβ8.2, the overall binding site of mVβ8.2-SEG is in close agreement with those previously described in the mVβ8.2-SEC2, mVβ8.2-SEC3, mVβ8.2-SEB, and mVβ8.2-SPEA complexes (17, 18, 19). However, detailed interactions at the interface are different, as described below.

The buried surface for mVβ8.2-SEG is 1285 Å^2, with equal contributions from both molecules. This value is within the range observed in other mVβ8.2 complexes with *S. aureus* SAgs (17, 18). By contrast, the complex of mVβ8.2 bound to *S. pyogenes* SAg SPEA displays a higher buried surface (1324 Å^2) because SPEA also contacts the CDR1 loop of Vβ (19). The SEG-MHC-II complex has not been crystallized, but sequence and structural alignment of SEG (33) with SEB, the only SAg of the family crystallized in complex with DR1 (11), showed that the putative binding site is conserved and adjacent to the TCR-binding site.

Structure of mVβ8.2-SEG Interface—The "hot spot" residues identified in SEB and SEC3 (24) that make the greatest energetic contribution to stabilization of the mVβ8.2-SAg complex (Asn-24, Tyr-88, and Gln-206; SEG numbering), as well as the energetically less important Asn-58, are strictly conserved in SEC1–3, SEB, SSA, and SPEA. The residues at

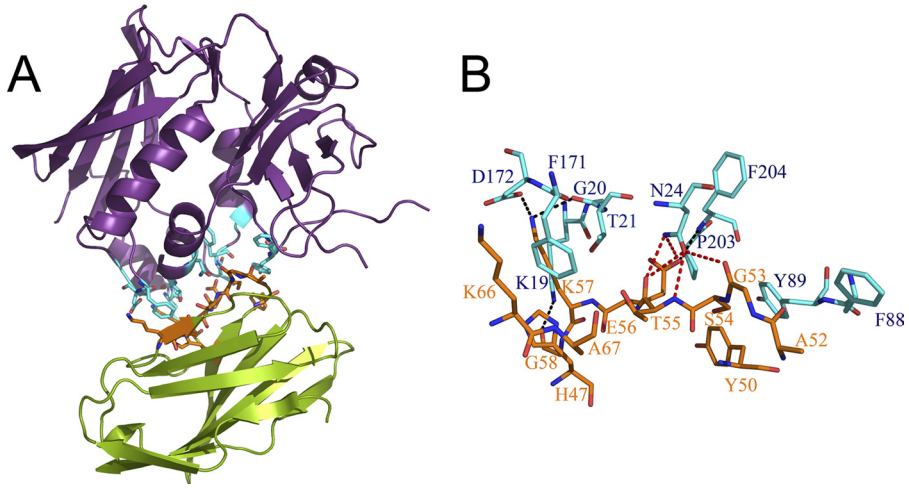

FIGURE 1. **Structure of the mVβ8.2-SEG complex.** *A*, overall structure of the mVβ8.2-SEG complex. Colors are as follows: mVβ is *green*, and SEG is *violet*. Residues of mVβ and SEG involved in the interaction are colored *orange* and *cyan*, respectively. *B*, interactions in the mVβ8.2-SEG interface. Nitrogen and oxygen atoms are colored *blue* and *red*, respectively. Hydrogen bonds are shown as *red dashes* when Asn-24^{SEG} is involved or as *black dashes*. mVβ8.2 residues are labeled in *orange*, and SEG residues are labeled in *blue*.

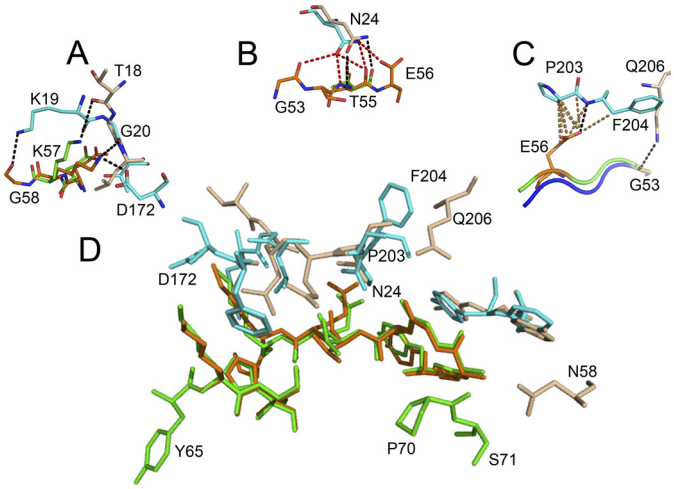

FIGURE 2. **Comparison of the mVβ8.2-SEG and mVβ8.2-SEB complex interfaces.** Residues of mVβ8.2 involved in the interaction with SEG or SEB are colored *orange* or *green*, respectively. SEG residues are colored *cyan*, and SEB residues are *beige*. Only the residues with differential features have been labeled for clarity. *A*, detail of the SAg α1α2 loop interaction. The insertion present in SEG allows the interaction with Gly-58$^{\beta}$. Hydrogen bonds are shown as *black dashes*. *B*, hydrogen bonds established between Asn-24^{SAg} and Vβ residues. Asn-24^{SEG} hydrogen bonds are *red dashes*, and Asn-24^{SEB} hydrogen bonds are *black dashes*. *C*, detail of the interaction between Pro-203^{SEG} and Phe-204^{SEG} with mVβ8.2. Hydrogen bonds are shown as *black dashes*, and van der Waals contacts are shown as *gold dashes*. *D*, superposition of the two mVβ8.2-SAg complex interfaces.

TABLE 2
mVβ8.2-SAg interactions
SEG numbering was used. mVβ8.2 and L2CM numbering correspond to the previously deposited sequences. mVβ8.2 and L2CM in Protein Data Bank codes 3MC0 (mVβ8.2) and 3OWE (L2CM) were numbered consecutively.

Hydrogen bonds			
β	SEG	SEB	SEC3
Gly-53 O	Asn-24 Oδ1	Gln-206 Nϵ2	Gln-206 Nϵ2
Thr-55 N	Asn-24 Oδ1	Asn-24 Oδ1	Asn-24 Oδ1
Thr-55 O	Asn-24 Oδ1	Asn-24 Nδ2	Asn-24 Nδ2
Thr-55 O	Asn-24 Nδ2		Thr-18 Oγ1
Glu-56 Oϵ1	Asn-24 Nδ2		
Glu-56 Oϵ1	Phe-204 N		
Lys-57 Nζ	Asp-172 Oδ1	Thr-18 O	
Lys-57 Nζ	Gly-20 O		
Gly-58 O	Lys-19 Nζ		
Pro-70		Asn-58 Nδ2	Asn-58 Nδ2
van der Waals contacts			
β	SEG	SEB	SEC3
His-47	Phe-171	Leu-21	
		Phe-171	
Tyr-50	Tyr-89	Tyr-89	Val-89
	Pro-203		
Gly-51			Val-89
Ala-52	Phe-88	Tyr-88	Tyr-88
Gly-53		Asn-24	Asn-24
			Tyr-27
			Gln-206
Ser-54	Asn-24	Asn-24	Asn-24
	Tyr-89		Val-89
	Asn-24	Leu-21	Thr-21
Thr-55	Phe-171	Asn-24	Asn-24
		Glu-23	
		Phe-171	
Glu-56	Pro-203	Leu-21	Thr-21
	Phe-204	Asn-24	
Lys-57	Thr-21	Gly-17	Gly-17
	Asp-172	Leu-21	Thr-21
Gly-58	Lys-19		
Tyr-65		Phe-171	
Lys-66	Phe-171	Phe-171	Phe-171
Ala-67	Phe-171	Phe-171	Phe-171
Pro-70		Asn-58	Leu-56
Ser-71		Asn-58	Asn-58

positions 21, 27, 89, and 171, despite not being conserved throughout the SEB family, form part of the mVβ8.2 binding interface on the SAgs with less energetic contribution (9, 14, 24). The binding surface formed by all these residues is shared by the mVβ8.2-SEB, mVβ8.2-SEC2, mVβ8.2-SEC3, and mVβ8.2-SPEA complexes and thus are characteristic of group II SAgs for binding to mVβ8.2. However, SEG displays a substantially different binding surface. SEG uses 10 residues in the interaction with mVβ8.2: Phe-88 and Tyr-89 of the small domain, and Lys-19, Gly-20, Thr-21, Asn-24, Phe-171, Asp-172, Pro-203, and Phe-204 of the large domain (Fig. 1*B*). Five of these positions (21, 24, 88, 89, and 171), but not strictly the residues at each of them, correlate with those of SEB, SEC2–3, and SPEA interacting with mVβ8.2. Only the residue at position 24 (Asn) that contacts mVβ8.2 is strictly conserved in all five SAg complexes, as well as in all SAgs of the SEB family (33). SEG does not use residues 27, 58, and 206 in the interaction, as the other SAgs do, but uses Lys-19 and Gly-20 (both absent in the other SAgs), Asp-172 and Pro-203 (not conserved), and Phe-204 (present in all the SAgs of the SEB family). Residues at these positions do not contact mVβ8.2 in any other of the four complexes. These SEG residues can interact with mVβ8.2 due to insertions of three and one residues in the α1–α2 and β11–η2 loops of SEG, respectively (33). The hydrogen bonds established between these two loops and FR3 of mVβ8.2 are mostly between the main chain of the SAg and side chains of the TCR (Fig. 1*B*). Altogether, these SEG residues contribute 30% of the total hydrogen bonds and several van der Waals contacts to the interface.

SEG displays an insertion of three residues in the α1α2 loop, which is absent in SEB, SEC3, and SPEA, promoting an interaction between FR3 Gly-58$^{\beta}$ and Lys-19^{SEG} through an extra hydrogen bond and additional van der Waals contacts (Fig. 2*A*), which are possible due to a conformational change in the Lys-19^{SEG} side chain after binding. In addition, Gly-20^{SEG} and Asp-172^{SEG} contribute with two extra hydrogen bonds to the interaction with FR3. These interactions are absent in the other complexes. Asn-24, which is conserved throughout the SEB family, makes five hydrogen bonds in SEG-mVβ8.2, compared with two in the SEB-mVβ8.2 and SEC3-mVβ8.2 complexes (Fig. 2*B*). The orientation of Pro-203^{SEG} and Phe-204^{SEG} allows the formation of several van der Waals contacts and a hydrogen bond with Glu-56$^{\beta}$, which are absent in the other complexes (Fig. 2*C* and Table 2).

The mVβ8.2 residues in contact with SEG are as follows: His-47 (FR2), Tyr-50, Ala-52, Gly-53, Ser-54, and Tyr-55 (CDR2); Glu-56, Lys-57, Gly-58, Lys-66, and Ala-67 (FR3) (Fig. 1*B*). FR2, CDR2, and FR3 contribute 2, 39, and 59% of the total contacts to SEG, respectively. FR3 makes the largest contribution to the interaction with SEG, which is a major difference with SEB-mVβ8.2 and SEC2–3-mVβ8.2 as, in these complexes, CDR2 accounts for 50 and 63%, respectively, of the total contacts to the SAg (9). A comparison of the mVβ8.2-SEG and mVβ8.2-SEB complex interfaces is shown in Fig. 2*D*. The SAg interaction with Pro-70$^{\beta}$ and Ser-71$^{\beta}$ (HV4) is highly conserved in the four other complexes (14, 17,

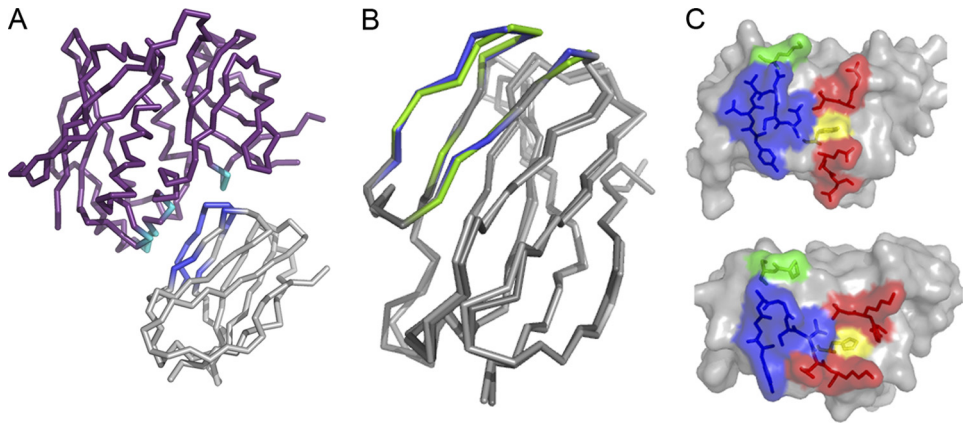

FIGURE 3. **Comparison of mouse Vβ structures stimulated by SEG.** *A*, superposition of mVβ7 structure (*white*) onto SEG (*purple*)-mVβ8.2 complex. The putative binding site is colored *cyan* (SEG) and *blue* (mVβ7). *B*, comparison of the mVβ8.2 (*gray*) and mVβ7 (*white*) structures. *C*, putative molecular surface of mVβ7 buried by SEG or SEB (*upper panel*), canonic mVβ8.2 surface buried by SAgs of group II, except SEG (*lower panel*). The FR2, FR3, CDR2, and HV4 involved in the interaction are colored *yellow*, *red*, *blue*, and *green*, respectively.

18). Pro-70$^{\beta}$ contributes to the complex stabilization with a hydrogen bond to Asn-58^{SAg} in the β2–β3 loop. This residue is strictly conserved among SAgs of the SEB family except in SEG, which has a Ser in this position. However, SEG has a deletion of three amino acids in the β2–β3 loop, which positions Ser-58^{SEG} (Asn-58^{SEB}) away from the interacting surface with mVβ8.2 (Fig. 2*D*). Structural superposition revealed 3.5–5.3 Å r.m.s. deviations with the other SAgs in this loop.

The 9 hydrogen bonds in the mVβ8.2-SEG complex (Fig. 1*B*) could explain the higher affinity of this interaction compared with the mVβ8.2-SEB and mVβ8.2-SEC2–3 complexes, which only have five hydrogen bonds (17, 18). However, the mVβ8.2-SPEA complex has 11 hydrogen bonds with an affinity similar to the latter complexes and lower than the mVβ8.2-SEG complex (19). The higher affinity of the mVβ8.2-SEG complex could be explained by the hydrogen bonding network around Asn-24^{SEG} (Fig. 2*B*). This network is not observed in the other three complexes, even though Asn-24^{SAg} is strictly conserved among bacterial SAgs reactive with mVβ8.2 and is present in most of the known SAgs. This residue was shown to be the major energetic hot spot in binding mVβ8.2 (24). On average, the Asn-24^{SAg} buried surface is 48 Å^2 in the other three complexes (range 47–54 Å^2), whereas in the mVβ8.2-SEG complex, the buried surface of this critical residue is 63 Å^2.

When free mVβ8.2 was superimposed onto mVβ8.2 in complex with SEB, SEC2–3, or SPEA, r.m.s. differences of 0.30, 0.31, and 0.56 Å, respectively, were obtained for all α carbon atoms. Free mVβ8.2 and mVβ8.2 bound to SEG superposed with an r.m.s. difference in α carbon positions of 0.41 Å. The most significant conformational change occurs at Glu-56$^{\beta}$, whose side chain shows an r.m.s. displacement of 0.86 Å. This movement is essential to contact Asn-24^{SEG} and Phe-204^{SEG} through hydrogen bonds (Fig. 2, *B* and *C*), which are not present in the other complexes.

Group II SAgs SEB, SEC3, and SPEA engage mVβ8.2 mostly through a conformation-dependent mechanism that is independent of specific Vβ amino acid side chains (9, 14, 17). However, the SEG-mVβ8.2 complex involves both main and side chains in the hydrogen bond interactions, suggesting a combination of two mechanisms, one conformation-dependent and the other sequence-dependent. Even though the interaction through side chains promotes specificity, this mechanism restricts the Vβ repertoire that can interact with the SAg.

Structural Basis for mVβ8.2 Binding Specificity of SEG—We previously described the *in vivo* selective expansion of murine T-cell subpopulations whereby SEG stimulates T-cells carrying Vβ7 and Vβ9 TCRs in a conventional manner. Surprisingly, we also found that SEG produces an earlier, stronger, and widespread stimulation of mVβ8.2 T-cells, compared with other members of SEB family, which reach a maximum at day 2 instead of day 4 or later as for SEC3 or SEB (30–32). The structure of SEG in unbound form (33) suggested a non-conventional binding site for mVβ8.2 and SEG, but it could not explain by itself the particular behavior of T-cells bearing mVβ8.2 when they are stimulated by SEG. To clarify this issue, the mVβ7 structure (Protein Data Bank code 3HE7) (40) was superposed onto the mVβ8.2-SEG complex using the program Lsqkab from the CCP4 program suite (Fig. 3*A*). The r.m.s. difference in α carbon positions for the 12 residues in the SEG binding site is only 0.43 Å (Fig. 3*B*). The putative residues involved in the binding surface were analyzed with the program Contact (CCP4 program suite), which showed that Asn-24^{SEG} would not be able to form the network of five hydrogen bonds as in the mVβ8.2-SEG complex. The interaction of Asn-58^{SAg} with Pro-70$^{\beta}$ and Ser-71$^{\beta}$ (HV4) is highly conserved in the mVβ8.2-SAg binding site. As described above, SEG does not contact mVβ8.2 HV4 due to a three-residue insertion in the β2–β3 loop, such that Ser-58^{SEG} is not present in the interface of mVβ8.2-SEG complex. However, in the mVβ7-SEG complex, SEG uses Tyr-59^{SEG} of the β2–β3 loop and Ser-31^{SEG} to contact Val-52$^{\beta7}$ (CDR2) and Lys-70$^{\beta7}$ (HV4), respectively (Fig. 3*C*). In the interaction with mVβ8.2, SEG uses three new residues, Asp-172, Pro-203, and Phe-204. Strikingly, residues 172, 203, and 204 are not part of the binding site in the mVβ8.2-SEB, mVβ8.2-SEC3, or the putative mVβ7-SEG complex.

SEB also interacts with mVβ7. When mVβ7 was superposed onto the mVβ8.2-SEB complex and the putative bind-

ing site, mVβ7-SEB did not differ from the mVβ8.2-SEB surface interaction (Fig. 3*C*). This analysis suggests that SEG contains a binding site for mVβ7 similar to the site found in the other members of the SEB family with mVβ8.2 and with the others Vβ that these SAgs bind (9).

Structure of L2CM-SEG Interface—We also determined the structure of the L2CM-SEG complex to 2.6 Å resolution. L2CM is a variant of mVβ8.2 with 1500-fold higher affinity for SEC3 (34, 37). L2CM also displays higher affinity than Vβ8.2 for other members of SEB family, such as SSA (340-fold). By contrast, L2CM showed only a 2.5-fold increase in its affinity for SEG (33). The structure of the L2CM-SEG complex shows substantial difference with the L2CM-SEC3 interface.

L2CM contains 9 mutations, G17E/A52V/S54N/K66E/Q72H/E80V/L81S/T87S/G96V, but five of them (G17E, E80V, L81S, T87S, and G96V) are outside of the binding site. The other four increase affinity by cooperative or additive interactions (34, 37). The A52V mutation results in the addition of two methyl groups (Cγ1 and Cγ2 atoms) beyond the single methyl group of the wild-type side chain. These methyl groups increase the buried hydrophobic surface with SEG, as in the case of SEC3, which can account for the increase in affinity of L2CM for SEG, compared with mVβ8.2 for SEG. An analysis of the K66E mutation is more complicated because this mutation could positively or negatively affect the affinity in the presence of a second mutation (E80V). Because the binding site of mVβ8.2-SEG is conserved in that region, these mutations may have the same effect in both complexes. In wild-type mVβ8.2, Ser-54$^{\beta}$ makes an intramolecular hydrogen bond with Glu-56$^{\beta}$, precluding the interaction of this residue with the SAg. The mutation S54N promotes a water-mediated hydrogen bonding network that links the Asn-54$^{\beta}$ and Glu-56$^{\beta}$ side chains to main chain atoms of Lys-204^{SEC3}. In wild-type mVβ8.2-SEG, this interaction already exists because SEG exhibits a cleft in the β11–η2 region that allows interactions with the TCR (Fig. 2*C*). The TCR HV4 region is deeply involved in interactions with SAgs of the SEB family, except in the mVβ8.2-SEG complex. The mutation Q72H in HV4 favors the interaction between SEC3 and L2CM. Because SEG does not interact with mVβ8.2 or L2CM HV4 regions, this mutation does not affect its affinity for L2CM. The fact that just one of the nine L2CM mutations, A52V, has a positive effect on mVβ8.2-SEG binding could explain the small increase in affinity that SEG displays for L2CM.

Conclusions—The mVβ8.2 binding surfaces of SEB, SEC2–3, and SPEA, determined by x-ray crystallography of the corresponding complexes, and the putative SSA binding surface, predicted based on the structure of the unbound SAg (7, 14, 17, 18, 41), show conservation of most of the eight contacting residues that constitute the functional epitope. Several of those residues have being identified as hot spots because of their energetic contribution to binding (24). The SEG structure showed that the putative binding surface formed by the eight residues is discontinuous and revealed difference in three of the hot spots, Asn-58, Tyr-88, and Gln-206, which have been replaced by Ser-58, Phe-88, and Pro-206, respectively. Nevertheless, SEG displays the highest affinity described for mVβ8.2 (33). The mVβ8.2-SEG complex revealed that the surface facing mVβ8.2 includes residues Lys-19, Gly-20, Thr-21, Asn-24, Phe-88, Tyr-89, Phe-171, Asp-172, Pro-203, and Phe-204, constituting a continuous surface, which shows a shift in the binding site compared with other SEB family members (Fig. 4*A*). SEG mostly interacts with CDR2 and FR3 of mVβ8.2, but it shows no interaction with HV4 of mVβ8.2, which is highly conserved through the SEB family (Fig. 4*B*).

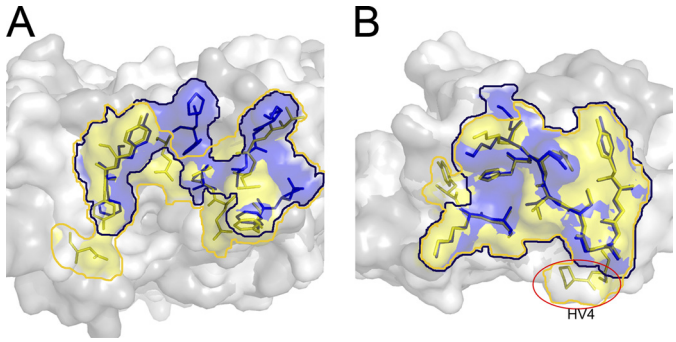

FIGURE 4. **The interacting surfaces of SAgs and mVβ8.2.** *A*, outline of the mVβ8.2 binding site of SEG (*thick blue line*) and SEB (*thick yellow line*) are superimposed on the surfaces of SEG (*white*) and SEB (*gray*) superimposed. *B*, the outline of SEG (*thick blue line*) and SEB (*thick yellow line*) binding sites are superimposed on the surfaces of mVβ8.2 bound to SEG (*white*) or SEB (*gray*) superimposed.

Until now, it was thought that those SAg residues making the greatest energetic contribution to stabilizing the mVβ8.2-SAg complexes were strictly conserved among enterotoxins reactive with mVβ8.2, thereby providing a basis for understanding why SAgs having other residues at these positions show different Vβ-binding specificities. The mVβ8.2-SEG structure allowed us to unambiguously characterize the interaction interface, showing that the hot spot residues are not totally conserved. SEG certainly stimulates T-cells bearing mVβ8.2 in an unconventional way as the other members of the family do, and the interaction with mVβ8.2 is characterized by the highest affinity. On the basis of these results, we conclude that the residues shared by SEG and the other members of the group II are essential for mVβ8.2 recognition, whereas the other residues involved in the interaction are responsible for the increased affinity. Thus, highly efficient activation of TCRs by SAgs could have an evolutionary basis and may be achieved through differential structural strategies of TCR binding, as described here.

Acknowledgments—Data for this study were measured at beamline X25 of the National Synchrotron Light Source.

REFERENCES

1. Fraser, J. D., and Proft, T. (2008) *Immunol. Rev.* **225,** 226–243
2. Lappin, E., and Ferguson, A. J. (2009) *Lancet Infect. Dis.* **9,** 281–290
3. Swaminathan, S., Furey, W., Pletcher, J., and Sax, M. (1992) *Nature* **359,** 801–806
4. Schad, E. M., Zaitseva, I., Zaitsev, V. N., Dohlsten, M., Kalland, T., Schlievert, P. M., Ohlendorf, D. H., and Svensson, L. A. (1995) *EMBO J.* **14,** 3292–3301
5. Papageorgiou, A. C., Acharya, K. R., Shapiro, R., Passalacqua, E. F., Brehm, R. D., and Tranter, H. S. (1995) *Structure* **3,** 769–779

6. Roussel, A., Anderson, B. F., Baker, H. M., Fraser, J. D., and Baker, E. N. (1997) *Nat. Struct. Biol.* **4,** 635–643
7. Sundberg, E., and Jardetzky, T. S. (1999) *Nat. Struct. Biol.* **6,** 123–129
8. Papageorgiou, A. C., Collins, C. M., Gutman, D. M., Kline, J. B., O'Brien, S. M., Tranter, H. S., and Acharya, K. R. (1999) *EMBO J.* **18,** 9–21
9. Li, H., Llera, A., Malchiodi, E. L., and Mariuzza, R. A. (1999) *Annu. Rev. Immunol.* **17,** 435–466
10. Brouillard, J. N., Günther, S., Varma, A. K., Gryski, I., Herfst, C. A., Rahman, A. K., Leung, D. Y., Schlievert, P. M., Madrenas, J., Sundberg, E. J., and McCormick, J. K. (2007) *J. Mol. Biol.* **367,** 925–934
11. Jardetzky, T. S., Brown, J. H., Gorga, J. C., Stern, L. J., Urban, R. G., Chi, Y. I., Stauffacher, C., Strominger, J. L., and Wiley, D. C. (1994) *Nature* **368,** 711–718
12. Li, Y., Li, H., Dimasi, N., McCormick, J. K., Martin, R., Schuck, P., Schlievert, P. M., and Mariuzza, R. A. (2001) *Immunity* **14,** 93–104
13. Petersson, K., Håkansson, M., Nilsson, H., Forsberg, G., Svensson, L. A., Liljas, A., and Walse, B. (2001) *EMBO J.* **20,** 3306–3312
14. Sundberg, E. J., Li, Y., and Mariuzza, R. A. (2002) *Curr. Opin. Immunol.* **14,** 36–44
15. Fernández, M. M., Guan, R., Swaminathan, C. P., Malchiodi, E. L., and Mariuzza, R. A. (2006) *J. Biol. Chem.* **281,** 25356–25364
16. Malchiodi, E. L., Eisenstein, E., Fields, B. A., Ohlendorf, D. H., Schlievert, P. M., Karjalainen, K., and Mariuzza, R. A. (1995) *J. Exp. Med.* **182,** 1833–1845
17. Fields, B. A., Malchiodi, E. L., Li, H., Ysern, X., Stauffacher, C. V., Schlievert, P. M., Karjalainen, K., and Mariuzza, R. A. (1996) *Nature* **384,** 188–192
18. Li, H., Llera, A., Tsuchiya, D., Leder, L., Ysern, X., Schlievert, P. M., Karjalainen, K., and Mariuzza, R. A. (1998) *Immunity* **9,** 807–816
19. Sundberg, E. J., Li, H., Llera, A. S., McCormick, J. K., Tormo, J., Schlievert, P. M., Karjalainen, K., and Mariuzza, R. A. (2002) *Structure* **10,** 687–699
20. McCormick, J. K., Yarwood, J. M., and Schlievert, P. M. (2001) *Annu. Rev. Microbiol.* **55,** 77–104
21. Brocke, S., Hausmann, S., Steinman, L., and Wucherpfennig, K. W. (1998) *Semin. Immunol.* **10,** 57–67
22. Yarwood, J. M., Leung, D. Y., and Schlievert, P. M. (2000) *FEMS Microbiol. Lett* **192,** 1–7
23. Madakamutil, L. T., Maricic, I., Sercarz, E., and Kumar, V. (2003) *J. Immunol.* **170,** 2985–2992
24. Leder, L., Llera, A., Lavoie, P. M., Lebedeva, M. I., Li, H., Sékaly, R. P., Bohach, G. A., Gahr, P. J., Schlievert, P. M., Karjalainen, K., and Mariuzza, R. A. (1998) *J. Exp. Med.* **187,** 823–833
25. Munson, S. H., Tremaine, M. T., Betley, M. J., and Welch, R. A. (1998) *Infect. Immun.* **66,** 3337–3348
26. Jarraud, S., Peyrat, M. A., Lim, A., Tristan, A., Bes, M., Mougel, C., Etienne, J., Vandenesch, F., Bonneville, M., and Lina, G. (2001) *J. Immunol.* **166,** 669–677
27. Jarraud, S., Cozon, G., Vandenesch, F., Bes, M., Etienne, J., and Lina, G. (1999) *J. Clin. Microbiol.* **37,** 2446–2449
28. Banks, M. C., Kamel, N. S., Zabriskie, J. B., Larone, D. H., Ursea, D., and Posnett, D. N. (2003) *J. Infect. Dis.* **187,** 77–86
29. Becker, K., Friedrich, A. W., Lubritz, G., Weilert, M., Peters, G., and Von Eiff, C. (2003) *J. Clin. Microbiol.* **41,** 1434–1439
30. Fernández, M. M., De Marzi, M. C., Berguer, P., Burzyn, D., Langley, R. J., Piazzon, I., Mariuzza, R. A., and Malchiodi, E. L. (2006) *Mol. Immunol.* **43,** 927–938
31. MacDonald, H. R., Baschieri, S., and Lees, R. K. (1991) *Eur. J. Immunol.* **21,** 1963–1966
32. Renno, T., Attinger, A., Locatelli, S., Bakker, T., Vacheron, S., and MacDonald, H. R. (1999) *J. Immunol.* **162,** 6312–6315
33. Fernández, M. M., Bhattacharya, S., De Marzi, M. C., Brown, P. H., Kerzic, M., Schuck, P., Mariuzza, R. A., and Malchiodi, E. L. (2007) *Proteins* **68,** 389–402
34. Yang, J., Swaminathan, C. P., Huang, Y., Guan, R., Cho, S., Kieke, M. C., Kranz, D. M., Mariuzza, R. A., and Sundberg, E. J. (2003) *J. Biol. Chem.* **278,** 50412–50421
35. Otwinowski, Z., and Minor, W. (1997) *Methods Enzymol.* **276,** 307–326
36. Collaborative Computational Project, Number 4. (1994) *Acta Crystallogr. D Biol. Crystallogr.* **50,** 760–763
37. Cho, S., Swaminathan, C. P., Yang, J., Kerzic, M. C., Guan, R., Kieke, M. C., Kranz, D. M., Mariuzza, R. A., and Sundberg, E. J. (2005) *Structure* **13,** 1775–1787
38. McRee, D. E. (1999) *J. Struct. Biol.* **125,** 156–165
39. Murshudov, G. N., Vagin, A. A., and Dodson, E. J. (1997) *Acta Crystallogr. D Biol. Crystallogr.* **53,** 240–255
40. Pellicci, D. G., Patel, O., Kjer-Nielsen, L., Pang, S. S., Sullivan, L. C., Kyparissoudis, K., Brooks, A. G., Reid, H. H., Gras, S., Lucet, I. S., Koh, R., Smyth, M. J., Mallevaey, T., Matsuda, J. L., Gapin, L., McCluskey, J., Godfrey, D. I., and Rossjohn, J. (2009) *Immunity* **31,** 47–59
41. De Marzí, M. C., Fernández, M. M., Sundberg, E. J., Molinero, L., Zwirner, N. W., Llera, A. S., Mariuzza, R. A., and Malchiodi, E. L. (2004) *Eur. J. Biochem.* **271,** 4075–4083